



LAWRENCE  
LIVERMORE  
NATIONAL  
LABORATORY

# Mitigating Teleportation Error in Frequency Dependent Hybrid Implicit Monte Carlo Diffusion Methods

M. A. Cleveland, N. A. Gentile

December 23, 2013

Journal of Computational and Theoretical Transport

## **Disclaimer**

---

This document was prepared as an account of work sponsored by an agency of the United States government. Neither the United States government nor Lawrence Livermore National Security, LLC, nor any of their employees makes any warranty, expressed or implied, or assumes any legal liability or responsibility for the accuracy, completeness, or usefulness of any information, apparatus, product, or process disclosed, or represents that its use would not infringe privately owned rights. Reference herein to any specific commercial product, process, or service by trade name, trademark, manufacturer, or otherwise does not necessarily constitute or imply its endorsement, recommendation, or favoring by the United States government or Lawrence Livermore National Security, LLC. The views and opinions of authors expressed herein do not necessarily state or reflect those of the United States government or Lawrence Livermore National Security, LLC, and shall not be used for advertising or product endorsement purposes.

# Mitigating teleportation error in frequency dependent Hybrid Implicit Monte Carlo Diffusion methods

Mathew A. Cleveland\*, Nick Gentile

*Lawrence Livermore National Laboratory, L-405, P. O. Box 808, Livermore California 94550*

---

## Abstract

This work investigates teleportation error in frequency dependent Hybrid Implicit Monte Carlo Diffusion (HIMCD). HIMCD dynamically applies Implicit Monte Carlo Diffusion (IMD) [1, 2] to regions of a problem that are opaque and diffusive while applying standard Implicit Monte Carlo (IMC) [3] to regions where the diffusion approximation is invalid. Teleportation error arises in Monte Carlo simulations when a source is represented with the wrong spatial distribution causing radiation energy to propagate unphysically fast through a material [4]. Both frequency dependent HIMCD and Hybrid IMC/DDMC [5] suffer from a new source of teleportation error that is intrinsic to these methods. This teleportation error arises from sampling a new spatial location of a Monte Carlo particle when it scatters from a diffusive opaque group to a moderately opaque transport group. In this work we show that by sampling these “up-scatter” locations with a flat spatial distribution in the cell, as was done in previous work [5, 6], creates significant teleportation error in optically thick cells. We then show that source tilting can improve these results for moderately opaque cells, but is not accurate enough to significantly improve the teleportation error in extremely opaque cells. Finally we present a new set of criteria that can be used to define which opacity groups are diffusive, in conjunction with source tilting, to significantly reduce teleportation regardless of the cell’s opacity. We refer to this new set of diffusion criteria as “over-lumping” because it includes moderately opaque frequency groups, which were previously excluded by other criteria [5], into the diffusion domain. The over-lumping criteria is tested using two test cases: a Marshak wave moving through stationary optically thick iron, and a frequency-dependent radiation hydrodynamic ablation test case.

---

## 1. Introduction

Many radiation hydrodynamic problems, such as those found in astrophysics, are composed of strongly heterogeneous materials that can vary in optical thicknesses by many orders of magnitude. Hybrid Implicit Monte Carlo Diffusion (HIMCD) [7] and

---

\*Corresponding author. Tel + 1 925 422-0287; e-mail: cleveland7@llnl.gov  
LLNL-JRNL-NUMBER-DRAFT

*Preprint submitted to Elsevier*

*December 20, 2013*

Hybrid Discrete Diffusion Monte Carlo (DDMC) [6] can accurately resolve the radiation hydrodynamics equations more efficiently than the standard Implicit Monte Carlo (IMC) [3] approach typically used on these types of problems.

HIMCD couples IMC to Implicit Monte Carlo Diffusion (IMD) [1]. IMD evaluates a spatially discretized diffusion equation using a Monte Carlo technique. DDMC [5] differs primarily in the way that the photons are tracked in time. IMD tracks photon discretely in time based on the temporal discretization, and DDMC tracks photon continuously in time [2]. This work focuses on IMD but the reader should note that much of what is discussed is similarly applicable to DDMC. Similarly, many of the tools developed to implement this work were originally developed for DDMC and will be referenced as such.

It has been well documented that Implicit Monte Carlo methods can produce significant errors in simulations with optically thick material or small time steps [4, 8]. The error that arises in these simulations has been termed teleportation error. The term “teleportation error” was originally coined by McKinley et al. [4] to describe the unphysical propagation (or “teleportation”) of energy in a simulation. This teleportation of energy happens when using a poor representation of the shape of the emission source in a zone with a sharp temperature gradient. Figure 1 shows an example of different source shapes for an exponential temperature distribution. If Monte Carlo (MC) particle locations are determined using the piecewise constant temperature distribution, such as the red line in the first zone of Figure 1, an unphysical amount of energy can be placed near the colder zone. This teleportation error is unique to Monte Carlo methods because MC particles are tracked continuously in space, unlike deterministic methods that are discrete in space. Using asymptotic analysis Densmore [8] confirmed, what was shown numerically by McKinley et al., that teleportation error from the piecewise constant representation of the emission source can be significant for small time steps in optically thick material.

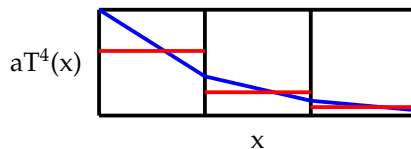


Figure 1: This figure shows a piecewise constant (depicted by the red lines) versus a linear continuous emission distribution (blue lines). For this example the exact emission profile was chosen as exponential. Using a piecewise constant representation of the temperature profile to sample emission locations places an unphysical amount of photon energy near the cold zone “teleporting” (or nonphysically propagating) energy forward in the simulation. This picture illustrates how the error in the piecewise constant is worse at strong gradients in the material temperature.

Densmore [8] showed that using a piecewise linear emission source distribution significantly reduces teleportation error in the IMC method. This treatment of the emissions source is commonly referred to as “source tilting” and is currently used in the IMC package of the Kull [9] multiphysics software suite.

In this work we show that frequency dependent HIMCD and DDMC create a previously neglected form of teleportation error. This error arises from the treatment of the IMD-to-IMC scattering source. Densmore actually used a simplified linear equation and

varied the shape of the scattering source to demonstrate the presence of teleportation error in the emission source representation of IMC. This is exactly how the error arises in the HIMCD and Hybrid DDMC method, however to the authors knowledge there has not been mention of this error, or how to mitigate it, in any of the previous work on these methods. Finally in this work we will show ways to mitigate this error using source tilting and a new approach that we refer to as “over-lumping”.

## 2. Frequency-dependent HIMCD

This work will detail the development of the frequency dependent Hybrid Implicit Monte Carlo Diffusion equations. This will include a general description of how the HIMCD equations are formed, with a detailed description of the frequency dependent interface conditions that have not previously been discussed at length. Much of this work will build from the large literature base of the IMD and DDMC methods. This includes the previous work on frequency dependent IMD [2], frequency dependent Hybrid DDMC [5], and more recent work with regards to HIMCD and Hybrid DDMC with regards to the radiation hydrodynamics equations [7, 6].

Frequency dependent HIMCD defines the radiation field over two discrete domains: a diffusion domain and a transport domain. Initially consider an arbitrary function of space, time, and frequency that we will call the diffusion criterion, that defines the diffusion domain.

$$\gamma(r, t, \nu) = \begin{cases} 1 & \text{if Diffusion} \\ 0 & \text{if Transport} \end{cases}$$

The diffusion criterion can be defined in different ways, and we will show later how these different ways can effect the accuracy and efficiency of the method. In HIMCD, IMD is used to evaluate the diffusion equation in the zones that make up the diffusion domain. We present the diffusion equation here in its multigroup form:

$$\begin{aligned} \frac{\partial E_g}{\partial t} + c\bar{\nabla} \cdot \frac{1}{3\kappa_g} \bar{\nabla} E_g - c\kappa_g f E_g - c\kappa_g E_g (1-f) &= \frac{\int_g^{g+1} b(\nu, t) \kappa_g \gamma_g d\nu}{\kappa_p} \kappa_p f a c T^4 \\ + \frac{\int_g^{g+1} b(\nu, t) \kappa_g \gamma_g d\nu}{\kappa_p} \sum_{g=0}^N \kappa_g E_g \gamma_g (1-f) d\nu' & \\ + \frac{\int_g^{g+1} b(\nu, t) \kappa_g \gamma_g d\nu}{\kappa_p} \sum_{g=0}^N \int_0^{4\pi} \kappa_g I_g (1-\gamma_g) (1-f) d\bar{\Omega} & \quad (1) \end{aligned}$$

where the subscript  $g$  expresses a value that has been integrated over a single group's frequency range ( $\nu_g \leq \nu \leq \nu_{g+1}$ ),  $E_g = \int_g^{g+1} E_\nu d\nu$  is the group energy density,  $\kappa_g$  is the group opacity,  $\kappa_p = \int_0^\infty b(\nu, T) \kappa_\nu d\nu$  is the Planck opacity,  $b(\nu, T)$  is the normalized Planck distribution,  $f$  is the fleck factor,  $a$  is the radiation constant, and  $c$  is the speed of light. At this point the only unique part of the HIMCD diffusion equation is the presence of the diffusion criterion that determines how much of each source is attributed to the diffusion groups. Eq. 1 also has an effective scattering source that accounts for photons scattered from the transport frequency ( $\gamma_g = 0$ ) in a zone to the diffusion frequencies ( $\gamma_g = 1$ ).

IMC is used to evaluate the transport equation in the remainder of the domain.

$$\begin{aligned}
\frac{1}{c} \frac{\partial I_g}{\partial t} + \bar{\Omega} \cdot \bar{\nabla} I_g + \kappa_g I_g &= \frac{1}{4\pi} \frac{\int_g^{g+1} b(\nu, T) \kappa_g (1 - \gamma_g) d\nu}{\kappa_p} \kappa_p f a c T^4 \\
&+ \frac{1}{4\pi} \frac{\int_g^{g+1} b(\nu, T) \kappa_g (1 - \gamma_g) d\nu}{\kappa_p} \sum_{g=0}^N \int_0^{4\pi} \kappa_g I_g (1 - \gamma_g) (1 - f) d\bar{\Omega}' \\
&+ \frac{1}{4\pi} \frac{\int_g^{g+1} b(\nu, T) \kappa_g (1 - \gamma_g) d\nu}{\kappa_p} \sum_{g=0}^N \kappa_g E_g \gamma_g (1 - f). \tag{2}
\end{aligned}$$

The material energy balance is used to account for radiation exchange with the material:

$$\rho \frac{\partial \epsilon}{\partial t} = \left( \int_0^\infty \int_0^{4\pi} \kappa_\nu f I_\nu d\Omega d\nu + c \sum_{g=0}^N \kappa_g f E_g \right) - \kappa_p f a c T^4. \tag{3}$$

Eq. 1, 2, and 3 make up the fundamental multigroup HIMCD equations. These equations can be used directly in this form using the spatial and temporal discretization described by Cleveland et al. [2]. However, in their current form effective scattering between diffusion groups can still make highly scattering simulations very expensive to evaluate [5]. Densmore et al. showed that using the frequency integrated (or “lumped”) diffusion equation can eliminate the process of scattering between diffusion groups. This can significantly improve the performance of Hybrid DDMC or HIMCD. This was originally shown for monotonic decreasing opacities [5], and was recently pointed out to be extensible to arbitrary opacity functions [6]. Our work uses this frequency integration scheme, and we show how it is applied to arbitrary opacity distributions for HIMCD. Note that this approach is functionally equivalent to Densmore’s original approach to frequency integrated Hybrid DDMC [5] for monotonic opacity functions.

### 2.1. Frequency-integrated HIMCD

Our implementation of frequency integrated HIMCD maintains a fixed frequency group stencil for all materials regardless of where diffusion groups are located. Figure 2 shows an example of what the frequency group stencil can look like as a function of frequency space. Using this approach all diffusion groups share a group averaged opacity value while maintaining the individual diffusion structure. For example, in Figure 2 the blue colored groups in zone  $i - 1$  all share the same opacity values but maintain their own frequency space as indicated by the dotted lines. This provides an estimate of the frequency distribution of the radiation energy density and allows us to use the powerful Monte Carlo integration scheme to evaluate the arbitrary transport-diffusion frequency group interface conditions at zone faces. The down side to this approach is that it has an increased memory cost as compared to using a single frequency group to represent the diffusion domain and it could be potentially more expensive because the need to select a new frequency group every time an interaction event is sampled.

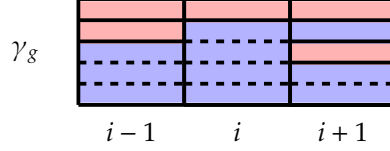


Figure 2: This figure shows an example of a frequency domain stencil for three adjoining zones. Each shaded section represents a frequency group, and its color coincides with either the diffusion (blue) or transport (red) domain, which is determined from its group diffusion criterion for that zone  $\gamma_g = \gamma(r, t, v_g)$ . The dotted lines in the blue regions help show that all diffusion groups in each zone are treated as a frequency integrated quantity. Furthermore we see that the frequency integrated diffusion domain can be discontinuous in frequency space (for example the frequency stencil of zone  $i + 1$ )

We begin by assuming that the frequency distribution of the energy density is Planckian [5] for all diffusion groups:

$$E_g^{n+1} \approx \tilde{E}^{n+1} \frac{\int_g^{g+1} b(v, T^n) \kappa_g \gamma_g dv}{\sum_{g'=0}^N \int_{g'}^{g'+1} b(v, T^n) \kappa_{g'} \gamma_{g'} dv} \equiv \tilde{E}^{n+1} \xi_g \quad (4)$$

where  $\xi_g$  is the diffusion group emission distribution and  $\tilde{E} = \int_0^\infty E_v \gamma_v dv$  is the frequency integrated diffusion energy density. Note that this frequency integrated quantity only includes the photon energy associated with diffusion groups (as determined by the frequency dependent diffusion criterion  $\gamma_v$ ). The opacity values are similarly weighted with a Planckian distribution:

$$\kappa_g = \tilde{\kappa}_p = \frac{\sum_{g'=0}^N \gamma_{g'} \kappa_{g'} \int_{g'}^{g'+1} b(v, T) dv}{\sum_{g'=0}^N \gamma_{g'} \int_{g'}^{g'+1} b(v, T^n) dv}. \quad (5)$$

It is necessary to define a weighted distribution for the reciprocal group opacity that will be used later to construct the diffusion opacity:

$$(\kappa_g)^{-1} = (\tilde{\kappa}_r)^{-1} = \left( \frac{\sum_{g'=0}^N \gamma_{g'} (\kappa_{g'})^{-1} \int_{g'}^{g'+1} \frac{db}{dT}(v, T) dv}{\sum_{g'=0}^N \gamma_{g'} \int_{g'}^{g'+1} \frac{db}{dT}(v, T^n) dv} \right). \quad (6)$$

This weighted reciprocal value is akin to a partial Rosseland mean opacity, as opposed to the Planck weighted reciprocal mean used by Densmore [5], because it is weighted using the derivative of the normalized Planck function  $\frac{db}{dT}(v, T)$ . We use the derivative Planck function for the reciprocal mean, as opposed to the normal Planck function, because it is known to produce more accurate results for frequency integrated diffusion.

Given the assumed function for the diffusion group energy density (Eq. 4) and the weighted diffusion group opacity (Eq. 5), it is possible to analytically account for the

effective scattering within diffusion groups (the 6th term in Eq 1):

$$\begin{aligned}
& \frac{\int_g^{g+1} b(v, t) \kappa_g \gamma_g dv}{\kappa_p} \sum_{g=0}^N \kappa_g E_g \gamma_g (1-f) dv' \\
= & \frac{\sum_g^N \int_{g'}^{g'+1} b(v, T^n) \kappa_{g'} \gamma_{g'} dv}{\kappa_p} \tilde{\kappa}_p \bar{E}^{n+1} \frac{\int_g^{g+1} b(v, T^n) \kappa_g \gamma_g dv}{\sum_{g'=0}^N \int_{g'}^{g'+1} b(v, T^n) \kappa_{g'} \gamma_{g'} dv} (1-f) \\
= & \frac{\sum_g^N \int_{g'}^{g'+1} b(v, T^n) \kappa_{g'} \gamma_{g'} dv}{\kappa_p} \tilde{\kappa}_p E_g (1-f) \\
\equiv & \alpha \tilde{\kappa}_p E_g (1-f) \tag{7}
\end{aligned}$$

where  $\alpha$  is the ratio of the radiation energy emitted into the diffusion groups. The multigroup diffusion equation (Eq. 1) can now be re-written given Eqs. 5, 6, and 7:

$$\begin{aligned}
\frac{\partial E_g}{\partial t} + c \bar{\nabla} \cdot \frac{1}{3 \bar{\kappa}_r} \bar{\nabla} E_g - c \tilde{\kappa}_p f E_g - c \tilde{\kappa}_p E_g (1-f)(1-\alpha) = \xi_g \alpha \kappa_p f a c T^4 \\
+ \xi_g \alpha \sum_{g=0}^N \int_0^{4\pi} \kappa_g I_g (1-\gamma_g) (1-f) \partial \bar{\Omega}. \tag{8}
\end{aligned}$$

Note that the effective scattering between diffusion groups has now been eliminated. This significantly improves the performance of the frequency dependent HIMCD method.

The multigroup HIMCD method with frequency integrated diffusion opacities is now formed by Eqs. 8, 2, and 3. Now it is necessary to chose a spatial and temporal discretization for the diffusion equation.

## 2.2. The discretized diffusion equation

IMD evaluates the diffusion equations by forming interaction probabilities from the spatial and temporal discretized diffusion equation. This work applies a finite volume central differencing spatial discretization and a backward Euler time discretization to Eq. 8. This is the same spatial and temporal scheme applied to the frequency-independent IMD equations by Cleveland et al. [7]. The discretized diffusion equation for a diffusion group  $g$  can be written for a single zone  $i$  with  $M$  diffusion-transport faces and  $J$  diffusion-diffusion faces:

$$\begin{aligned}
E_{g,i}^{n+1} \Delta V_i - c \sum_j^J \bar{n}_j \cdot D_{g,j} \nabla E_{g,j}^{n+1} \delta t \delta A_j - c \sum_m^M \int_A \int_{t^n}^{t^{n+1}} \bar{n}_m \cdot F_{g,m} dt \delta A_m + c \tilde{\kappa}_p f E_{g,i}^{n+1} \\
+ c \tilde{\kappa}_p E_{g,i}^{n+1} (1-f)(1-\alpha) = \xi_g \alpha \kappa_p f a c T^4 \Delta t \Delta V \\
+ E_{g,i}^n \Delta V_i + \xi_g \alpha \int_0^\infty \int_0^{4\pi} \kappa_v (1-f) I_v \partial \bar{\Omega}' \tag{9}
\end{aligned}$$

where  $\bar{n}$  is the unit normal of a zone face,  $D_g$  is the face based diffusion coefficient, and  $A$  is the face area. Coefficients associated with the transport-diffusion interface

faces (denoted by  $m$  subscript) are developed later in the diffusion-transport spatial interface condition and are therefore left in the integral form. The face averaged diffusion coefficient for a second order finite volume discretization applied to orthogonal meshes can be expressed as [10]:

$$D_{g,j} = \frac{D_{j^+} D_{j^-} (X_{j+\frac{1}{2}} - X_{j-\frac{1}{2}})}{D_{j^+} (X_j - X_{j-\frac{1}{2}}) + D_{j^-} (X_{j+\frac{1}{2}} - X_j)} \quad (10)$$

where  $X$  is a position in space. The subscripts  $(j + \frac{1}{2})$  and  $(j - \frac{1}{2})$  denote zone-centered values and the subscripts  $(j^+)$  and  $(j^-)$  denote the material property immediately on either side of face  $j$ .

The selection of the diffusion coefficients on either side of the face ( $D_{j^+}$  and  $D_{j^-}$ ) for this discretization scheme is important, because very thick zones can nonphysically stop photon propagation when adjoined by relatively thin zones [10]. In this work we evaluate the diffusion coefficient value at every face of every zone using the temperature at that face ( $T_j$ ).

$$D_{g,j^\pm} = \frac{1}{3\tilde{\kappa}_r(X_{j\pm\frac{1}{2}}, T_j)} \quad (11)$$

The HIMCD algorithm allows MC particles to explicitly transition between the diffusion and transport domain given the interface conditions that connect the domains.

### 2.3. Diffusion-transport interface conditions

Monte Carlo particles can easily be tracked by either the IMC or IMD tracking procedures and only require additional information sampling (location, direction, and time) when they transition from IMD to IMC. The IMD algorithm simply disregards the extra information when MC particles are transitioned from IMC to IMD.

The transitions between IMC and IMD particles are based on the temporal, spatial, and frequency interface conditions that couple the diffusion and transport domains together. The frequency dependent temporal and spatial interface conditions listed here are very similar to the frequency-independent interface conditions that have previously been developed for HIMCD [7]. These diffusion-transport interface conditions are expressed in terms of the frequency dependent diffusion criterion used to define the diffusion and transport domains.

#### 2.3.1. Diffusion-transport temporal interface conditions

The diffusion temporal interface condition for the diffusion domain is defined as:

$$\left. \begin{array}{l} \text{if } \gamma_g^{n-1} = 0 \\ \text{and } \gamma_g^n = 1 \end{array} \right\} E_g^n = \frac{1}{c} \int_0^{4\pi} I_g^n d\bar{\Omega}$$

and similarly for the transport domain:

$$\left. \begin{array}{l} \text{if } \gamma_g^{n-1} = 1 \\ \text{and } \gamma_g^n = 0 \end{array} \right\} I_g^n = \frac{1}{\Delta V} \frac{1}{4\pi} c E_g^n \Delta V.$$

These interface conditions allow the diffusion domain stencil to change as a function of time and account for how the energy is redistributed in a new domain. Here we

intentionally kept fractions that could be canceled out to show that, when energy in the diffusion domain is moved to the transport domain in a subsequent time step ( $\gamma_g^{n-1} = 1$  and  $\gamma_g^n = 0$ ), we are required to redistribute the energy density in angle ( $(4\pi)^{-1}$ ) and space ( $(\Delta V)^{-1}$ ). The assumption that the previous energy density  $E_g^n$  is equally distributed in space and angle should be accurate because we do not use diffusion in a zone unless it is opaque enough for the radiation to be isotropic.

### 2.3.2. The diffusion–transport spatial interface condition

We employ the diffusion transport interface condition originally developed by Densmore et al. [11] for an interface between IMC and DDMC. This interface condition is defined such that it will preserve an accurate emissivity at the interface regardless of zone size [11]. The emissivity is defined as the fraction of incident radiation that is not reflected back through the incident surface [12]. The original derivation was for frequency-independent radiation calculations and we present it here for the frequency integrated form of the interface condition.

The interface condition for a transport zone that adjoins the interface face  $m$  can be broken down into two parts: one accounts for the photon intensity that is entering the zone (where the cosine angle between the photon and the interface normal is  $\mu_m < 0$ ) and the other accounts for the photon intensity that leaves the zone ( $\mu_m > 0$ ). The angular flux ( $\mu I|_m$ ) entering the transport zone through the diffusion-transport interface face ( $m$ ) is defined such that (if  $\mu_m < 0$ ):

$$\begin{aligned} \mu I|_{\mu_m < 0} &= \frac{1}{A_m} \frac{1}{\Delta t} \frac{1}{2\pi} \frac{\mu}{\int_{-1}^0 \mu_m d\mu} c E_{m+\frac{1}{2}}^{n+1} C_m \Delta t A_m \\ &+ \frac{1}{2\pi} \frac{\mu}{\int_{-1}^0 \mu_m d\mu} \int_0^{2\pi} \int_0^1 P_{\text{ref},m}[\mu_m] \mu_m I_m d\mu d\theta. \end{aligned} \quad (12)$$

We have intentionally left fractions that can be canceled in these equations to show that it is necessary to sample the particle direction ( $(2\pi)^{-1}$  and  $\mu(\int_{-1}^0 \mu_m d\mu)^{-1}$ ), location ( $(A_m)^{-1}$ ), and time ( $(\Delta t)^{-1}$ ) when an IMC particle is transitioned to an IMD particle. Notice that it is not necessary to re-sample the particle's location or time when they are reflected back into the transport zone. These reflections are assumed to be instantaneous and occur where and when the IMC particle originally crossed the interface face  $m$ . The angular flux that leaves the transport zone through the interface face  $m$  is defined as (if  $\mu_m > 0$ ):

$$\mu I|_{\mu_m > 0} = (1 - P_{\text{ref},m}[\mu_m]) \mu_m I_m \quad (13)$$

The reflection probability has a constraint on both the scattering ratio ( $\omega$ ) and zone optical thickness ( $\tau$ ) to ensure  $1 \leq P_{\text{ref},m}[\mu] \leq 0$ . These constraints are wrapped into the definition of the diffusion criterion. We have defined two new variables: the diffusion interface leakage coefficient  $C_m$ :

$$C_m = \frac{P'_m}{4} \quad (14)$$

and the incident cosine angle-dependent reflection probability:

$$P_{\text{ref},m}[\mu_m] = (1 - P'_m) 2 \left(1 + \frac{3}{2} \mu_m\right) \quad (15)$$

where the associated multiplication factor  $(2(1+\frac{3}{2}\mu))$  arises from the asymptotic diffusion-limit interface condition.  $P'_m$  is defined such that it preserves the analytic emissivity  $\epsilon'$  and is a function of the diffusion interface zone's material properties and discretized mesh [11]:

$$P'_m = \frac{\epsilon' \beta_m}{\beta_m - \frac{4}{3} \epsilon' \tau_m}. \quad (16)$$

The remaining variables are defined in reference [11] as:

$$\epsilon' = \frac{4}{3} \frac{\sqrt{3(1-\omega)}}{1 + \lambda \sqrt{3(1-\omega)}} \quad (17)$$

$$\beta_m = \frac{3}{2} (1 - \omega_m) \tau_m^2 + \sqrt{3(1 - \omega_m) \tau_m^2 + \frac{9}{4} (1 - \omega_m)^2 \tau_m^4} \quad (18)$$

$$\tau_m = \tilde{\kappa}_r \bar{n}_m \cdot \overline{\Delta X} \quad (19)$$

$$\omega_m = \frac{\tilde{\kappa}_r - \tilde{\kappa}_p f_{m+\frac{1}{2}}}{\tilde{\kappa}_r} \quad (20)$$

where  $\lambda = 0.7104$  is the extrapolation distance and  $\mu = \bar{\Omega} \cdot \bar{n}$  is the cosine of the angle between the particle direction and the face unit normal  $\bar{n}$  (which points from the transport zone to the diffusion zone).  $\overline{\Delta X} = 2(\bar{X}_m - \bar{X}_{m+\frac{1}{2}})$  is two times the vector from the position of the zone center  $\bar{X}_{m+\frac{1}{2}}$  to the interface face center  $\bar{X}_m$ . We will refer to  $\omega_m$  as the scattering ratio. These variables are defined using the frequency averaged opacity values from the lumped diffusion equation.

The overall interface condition can be written as a composition of the intensity leaving and entering the transport zone through the interface face  $m$ :

$$\left. \begin{array}{l} \text{if } \gamma_i^n = 0 \\ \text{and } \gamma_{m-\frac{1}{2}}^n = 1 \end{array} \right\} \mu I|_m = \begin{cases} \mu I|_{\mu_m < 0} & \text{if } \mu_m < 0 \\ \mu I|_{\mu_m > 0} & \text{if } \mu_m > 0 \end{cases}$$

The diffusion interface condition can be constructed by integrating the transport interface condition over angle:

$$\left. \begin{array}{l} \text{if } \gamma_i^n = 1 \\ \text{and } \gamma_{m-\frac{1}{2}}^n = 0 \end{array} \right\} \int_A \int_{t^n}^{t^{n+1}} \bar{n}_m \cdot \bar{F}_m dt dA_m.$$

where

$$\int_A \int_{t^n}^{t^{n+1}} \bar{n}_m \cdot \bar{F}_m dt dA_m = \int_A \int_{t^n}^{t^{n+1}} \int_0^{2\pi} \left( \int_{-1}^0 \mu I|_{\mu_m < 0} + \int_0^1 \mu I|_{\mu_m > 0} \right) d\mu d\theta dt dA_m. \quad (21)$$

### 2.3.3. Diffusion-transport scattering interface

The scattering interface between the transport and diffusion domains is defined in the HIMCD equations through the scattering source. When MC particles scatter from the transport to the diffusion domain (we refer to this as a down-scatter), it is only

necessary to sample a new diffusion group from the diffusion emission distribution  $\xi_g$  (defined by Eq. 4):

$$E_g = \xi_g \alpha \sum_{g'=0}^N \int_{t^n}^{t^{n+1}} \int_0^{4\pi} \kappa_{g'} I_{g'} (1 - \gamma_{g'}) (1 - f) d\bar{\Omega} dt \quad (22)$$

Scattering from the diffusion to the transport domain (referred to as up-scattering) requires us to re-sample a new MC particle direction, frequency, time, and zone location.

$$I_g = \frac{1}{\Delta t} \frac{1}{\Delta V} \frac{1}{4\pi} \frac{\int_g^{g+1} b(v, T) \kappa_g (1 - \gamma_g) dv}{\kappa_p} \sum_{g=0}^N \kappa_g E_g^{n+1} \gamma_g (1 - f) \Delta t \Delta V \quad (23)$$

It turns out that the accuracy of the HIMCD method is strongly dependent on how these up-scattering locations are sampled. This is unique to the HIMCD and Hybrid DDMC method because it requires that we treat these events using a discrete function rather than continuously as is done in IMC. Densmore showed the effects of treating the IMC emission source with different spatial distributions; treating effective scattering discretely, rather than continuously as is done in IMC, will cause significant teleportation error. This is exactly what happens in this work, though to the authors knowledge it has not been previously discussed for these hybrid methods.

In the remainder of this section we will summarize the frequency-dependent HIMCD algorithm. This includes a detailed description of the additional sampling that occurs in the frequency-integrated HIMCD scheme as apposed to the frequency-independent HIMCD method.

#### 2.4. Applying frequency-dependent HIMCD to evaluate the radiation field

The frequency-dependent HIMCD package presented in this work was implemented in the Kull [9] multiphysics software package, which already contains a well documented IMC package [9]. The addition of frequency dependence to the HIMCD package only requires a few modifications to the original frequency-independent HIMCD algorithm [7]. At the beginning of the time step the diffusion criterion  $\gamma_{i,g}^n$  is evaluated to define the diffusion domain ( $\gamma_{i,g}^n = 1$ ). Given the frequency stencil defined by the diffusion criterion it is possible to develop the IMD matrix using the frequency integrated coefficients presented in this work. Remember that we maintain the frequency stencil and replace the individual diffusion group opacity values within a zone with a single frequency integrated value. This forms a standard multigroup diffusion matrix where each diffusion group has the same frequency integrated opacity values but can still have a unique transport-diffusion interface condition. This allows us to use the MC method to estimate the frequency-dependence, of both zone and face centered quantities. This also removes the events which account for scattering from one diffusion group to another. These scattering events can dominate the simulation time and do not provide a significant amount of additional accuracy. The probabilities are generated using the matrix that forms the left hand side of the discretized diffusion equation (Eq. 9). Greater detail on how these probabilities are developed can be found in reference [2]. IMC and IMD particles are exchanged during Monte Carlo particle tracking according to the previously defined interface conditions.

The frequency-integrated HIMCD algorithm requires two additional sampling processes not present in frequency-independent HIMCD [7]. The first is that we must sample a new diffusion frequency at the beginning of every IMD random-walk. This sampling arises from the Planck emission normalization defined in Eq. 4. This means that MC particles always have a unique frequency that defines their group. This allows for a simple straightforward evaluation of the frequency dependence at zone interfaces.

The scattering sources that appear in the frequency-integrated HIMCD equations are evaluated explicitly during the Monte Carlo process by allowing the MC particles to scatter between the transport and diffusion domain. Down-scattering from transport to diffusion is straightforward and requires no additional sampling. Up-scattering can account for a significant percentage of the overall energy sourced into the transport domain. This makes the HIMCD method very sensitive to the accuracy of the sampling used to redistribute the MC energy into the transport domain. We will show how the source shape used to distribute the up-scattering events in the zone can significantly affect the accuracy of HIMCD and Hybrid DDMC methods.

### 3. Reducing teleportation error using source tilting

We begin by defining the frequency dependent diffusion criterion that has been used in previous work [5, 6, 7].

$$\gamma_g = \begin{cases} 1 & \text{if } \omega_g \geq 0.9 \text{ and } \tau_g^{\min} \geq 4 \\ 0 & \text{else} \end{cases}$$

This frequency-dependent diffusion criterion adheres to the minimum constraints required to produce reflection probabilities that are bounded between 1 and 0 for the frequency-integrated diffusion transport interface (Eq. 15). The diffusion criterion is defined using each zone's minimum optical depth ( $\tau_g^{\min}$ ) and scattering ratio ( $\omega_g$ ). Though lower scattering ratio can be used to generate valid interface probability ranges, a 90% scattering ratio was chosen in this work so that transitions to diffusion occur only when diffusion is valid [11]. We evaluate this diffusion criterion for every zone at the beginning of every time step given the current mesh and material properties. The group scattering ratio is evaluated as:

$$\omega_g = \frac{\kappa_g - f\kappa_g}{\kappa_g} \quad (24)$$

The optical depth is defined as:

$$\tau_g^{\min} = \kappa_g \bar{n} \cdot \overline{\Delta X}_{\min} \quad (25)$$

where the vector  $\overline{\Delta X}_{\min} = 2(\bar{X}_f - \bar{X}_i)$  is two times the vector from the zone center  $\bar{X}_i$  to the closest zone face  $\bar{X}_f$ . This is an approximation of the minimum zone width. This conservative definition of the diffusion criterion ensures that the frequency-integrated opacity values:

$$\omega = \frac{\tilde{\kappa}_r - \tilde{\kappa}_p f}{\tilde{\kappa}_r} \quad (26)$$

and

$$\tau^{\min} = \tilde{\kappa}_r \bar{n} \cdot \overline{\Delta X}_{\min} \quad (27)$$

form bounded interface probabilities

To show the importance of source tilting we begin with a numerical demonstration of teleportation error in frequency-dependent HIMCD when up-scatter events are distributed equally within a zone.

### 3.1. A numerical demonstration of teleportation error and the effects of source tilting in HIMCD

In this work source tilting mitigates teleportation error that arises from sampling the spatial locations of the emission source. This type of emission source teleportation error in the IMC method is dominant in the presence of extremely optically thick zones when small time steps are taken [8]. To demonstrate the sensitivity of these hybrid methods to the spatial sampling of the up-scattering events we have chosen a problem that is dominated by effective scattering. The dominance of the effective scattering and source titling the emission source prevents teleportation error in the emission source from being a significant factor in the simulation.

We begin by showing a simple 1D Marshak wave problem which was originally presented in the work of Densmore et al. [5] to demonstrate the performance of frequency-integrated hybrid DDMC. This problem consists of a cold ( $T_0 = 1$  [eV]) heterogeneous semi-infinite slab of material with an analytic opacity that is dependent on temperature and frequency:

$$\kappa(\nu, T) = \frac{1000kT^{-0.5}}{(h\nu)^3}. \quad (28)$$

This material is heated by a blackbody emission source  $T = 1$  [keV] at  $x = 0$ . Figure 3 show the results at a simulation time of  $t = 1 \times 10^{-9}$  [sec] using a time step size of  $\Delta t = 1 \times 10^{-11}$  [sec] and a zone size of  $\Delta x = 0.02$  [cm]. This compares Hybrid DDMC and HIMCD to the solution evaluated using IMC and  $S_N$ . The HIMCD and IMC simulations were run in Kull using  $1 \times 10^5$  MC particles per time step. The IMC method uses source tilting for the emission source. The up-scattering events are distributed equally within a zone as was done in previous work [5, 6]. The  $S_N$  simulation was run in Kull using  $S_6$  level symmetric quadrature set. The Hybrid DDMC simulation was run in the Milagro [13] radiative transfer package at LANL.

These results show that the hybrid methods cause the material temperature to propagate (or "teleport") faster than the reference results obtained using IMC and  $S_N$ . This teleportation error arises from distributing the up-scattering events uniformly within each zone. This effect went unnoticed in the work for Densmore [5] and Wollaeger [6] because the very fine spatial mesh sizes masked the effect. Thanks to the moderate zone opaqueness, large time step sizes, and emission source titling the IMC simulation avoids the development of any significant teleportation error. This is not the case for the Hybrid methods because the problem is dominated by effective scattering which is being represented as a discrete, rather than continuous, event.

Similar to emission source teleportation error that arises in IMC, we would expect that the up-scatter source teleportation error would be reduced as the spatial mesh is refined. Figure 4 shows that as the spatial mesh is refined, the HIMCD method that distributes the up-scattering events uniformly in each zone converges to the reference  $S_N$  simulation.

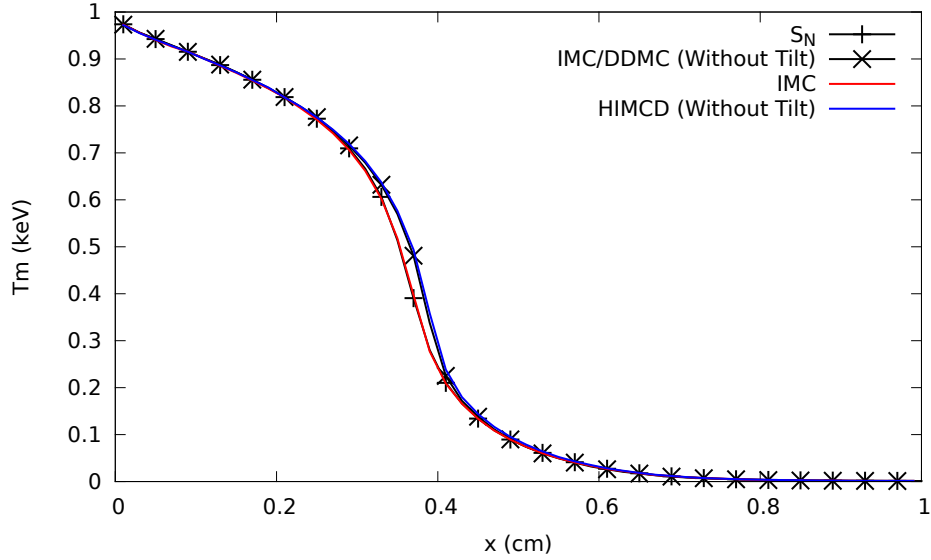


Figure 3: The material temperature profile evaluated by HIMCD, Hybrid DDMC, IMC, and  $S_N$ . This shows that the hybrid methods without source tilting result in a significant amount of overheating in the regions of strong temperature gradients.

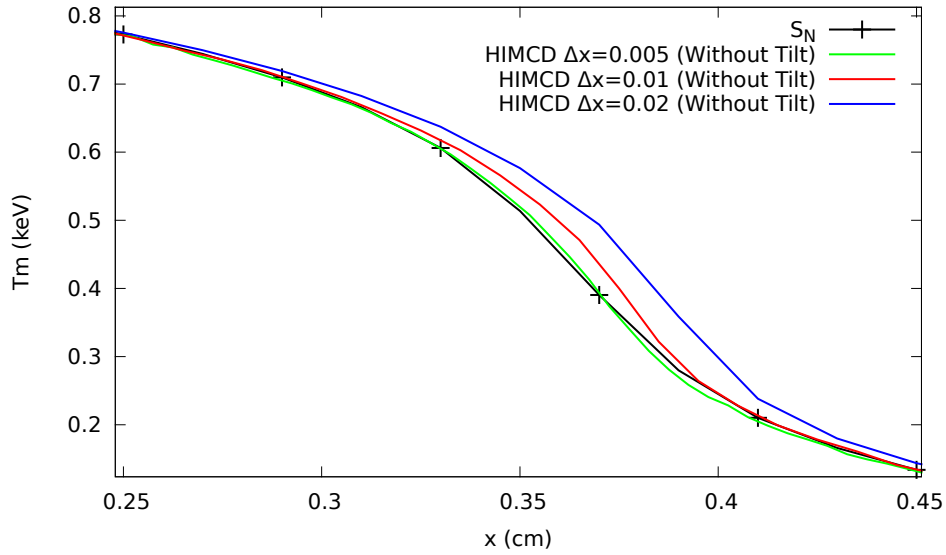


Figure 4: Refining the spatial mesh quickly reduces the teleportation error that arises in the HIMCD method. This is due in part to two effects: the first is the fact that as the zones are made smaller the assumption that the up-scattering events are equally distributed in space becomes more accurate, the second is that as the zones are made smaller fewer groups meet the diffusion criterion and more of the problem is treated directly with transport using IMC.

In the following section we will show that representing the spatial distribution of the up-scattering events with the same source tilting used for the IMC emission source significantly reduces the up-scattering teleportation error.

### 3.2. Mitigating up-scattering teleportation error using source tilting

An up-scatter event can be physically interpreted as a photon that is absorbed in a diffusion domain and then remitted in the transport domain during a single time step. This quickly leads to the assumption that the real spatial distribution of the up-scattering source may closely resemble that of the emission source. We therefore, apply the same source tilting scheme used to improve the spatial representation of the emission source to the up-scattering source.

The source tilting scheme used in the Kull IMC package relies on a simple linear interpolation of a weighted emission temperature  $T^4(X)$ , where the emission temperature is weighted with the Rosseland mean opacity. This weighted temperature field is evaluated at the zone faces and would be defined as:

$$T^4(X_f) = \frac{T^4(X_f)}{\kappa_r(X_f)} \bigg/ \sum_f^N \frac{1}{\kappa_r(X_{f'})} \quad (29)$$

for face  $f$  of a zone with  $N$  faces. The resulting sampling for the cumulative probability density function of the linear interpolation for a 1D zone is:

$$X = X_0 + (X_1 - X_0) \frac{(\sqrt{T_0^8 + m(T_1^8 - T_0^8)} - T_0^4)}{T_1^4 - T_0^4} \quad (30)$$

where  $m$  is a random number between 0 and 1.

Applying the source tilting scheme defined in Eq. 30 to the up-scattering source in the frequency-dependent HIMCD method significantly improves the results of the Marshak wave problem. Figure 5 show the improved results using source tilting to select the location of the up-scattering events. This is a significant improvement as compared to the results shown for the same coarse mesh size in Figure 4; however the up-scattering source tilting slightly under predicts the propagation of the material temperature wave.

### 3.3. Source tilting is not enough to completely prevent teleportation error

Even though using source titling to sample the up-scatter locations significantly improved the results of the Marshak wave problem, it is not enough to prevent teleportation error from becoming significant in all simulations. Consider an optically thick semi-infinite block of iron heated by a black body face source  $T = 1$  [keV] at  $x = 0$ . The slab of iron is given an initial temperature  $T_0 = 0.5$  [keV], and density of  $\rho_0 = 7.4$  [g/cc]. Figure 6 show the IMC simulation results at three different spatial refinements of the domain  $0 \leq x \leq 1$  at simulation time  $t = 1 \times 10^{-8}$  [sec] using a time step size of  $\Delta t = 10 \times 10^{-10}$  [sec]. Figure 6 shows that emission source tilting does not prevent teleportation error from becoming significant in the 10 zone simulation. We would expect HIMCD to produce significantly better results for the 10 zone test case, because the

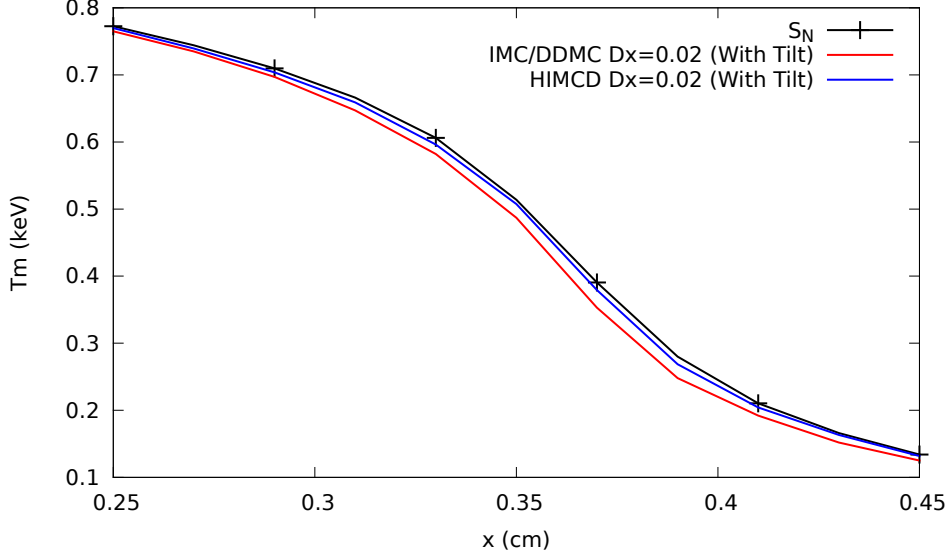


Figure 5: Source tilting at up-scattering events significantly improves the Hybrid DDMC and HIMCD results for the Marshak wave benchmark.

emission spectrum should be dominated by diffusion in optically thick material. Figure 7 shows the results of the HIMCD simulation at the same spatial refinements used in the IMC simulations. Figures 6 and 7 show that our tilting scheme is not accurate enough to completely prevent teleportation error from becoming significant. What is worse is that the Hybrid methods are less accurate in the intermediate refinement range where there is a significant amount of up-scattering.

We will now go on to show how an improved diffusion criterion can significantly reduce teleportation error in the Hybrid methods.

#### 4. An improved diffusion criterion to mitigate teleportation error

We assert that the dominant source of up-scattering teleportation error occurs during up-scattering from the diffusion domain to moderately opaque transport groups ( $0.01 \leq \tau_g^{\min} \leq 4$ ) that have previously been excluded by the diffusion criterion defined in Section 3. Previous definitions of the diffusion criterion were based only on frequency dependent values ( $\tau_g^{\min}$  and  $\omega_g$ ) even though they rely on frequency integrated quantities. The previous definition of the diffusion criterion was a conservative way to ensure that the frequency integrated transport-diffusion spatial interface condition produced probabilities between 0 and 1. Densmore et al. showed that the minimum zone optical depth  $\tau_{\min}$  can be determined from [14]:

$$\frac{3}{2}(1-\omega)\tau_{\min} + \sqrt{3(1-\omega) + \frac{9}{4}(1-\omega)^2\tau_{\min}^2} = \frac{\sqrt{3(1-\omega)}}{1 + (\lambda - \frac{5}{3})\sqrt{3(1-\omega)}} \quad (31)$$

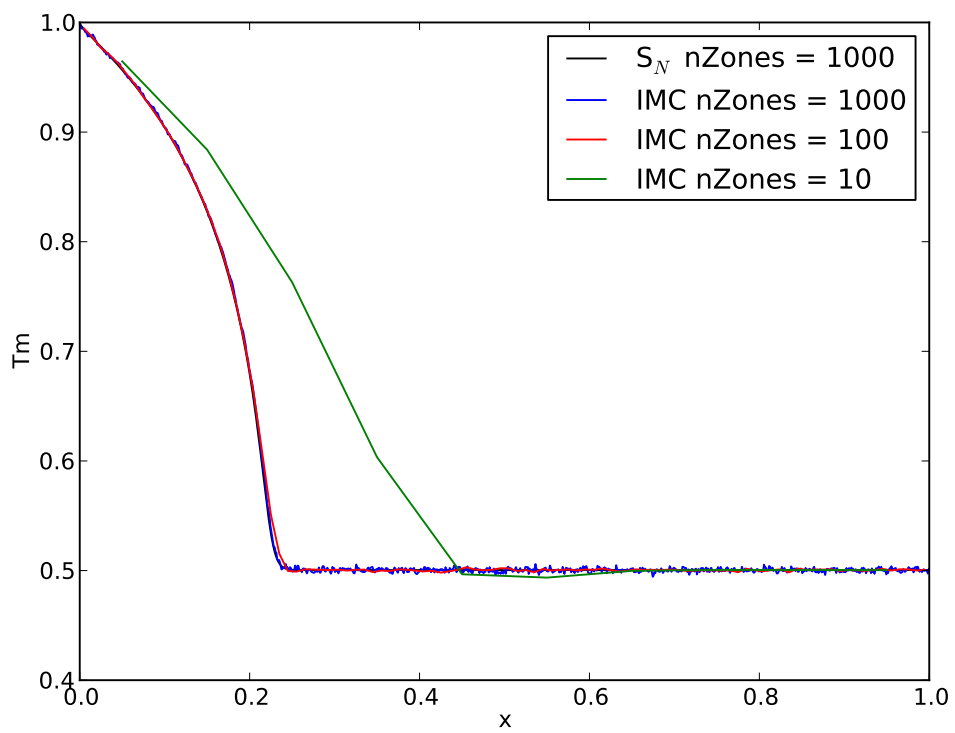


Figure 6: The IMC simulation results of the heated iron test case at three different spatial refinements. Even with source tilting the emission source teleportation error is very significant for the 10 zone simulation.

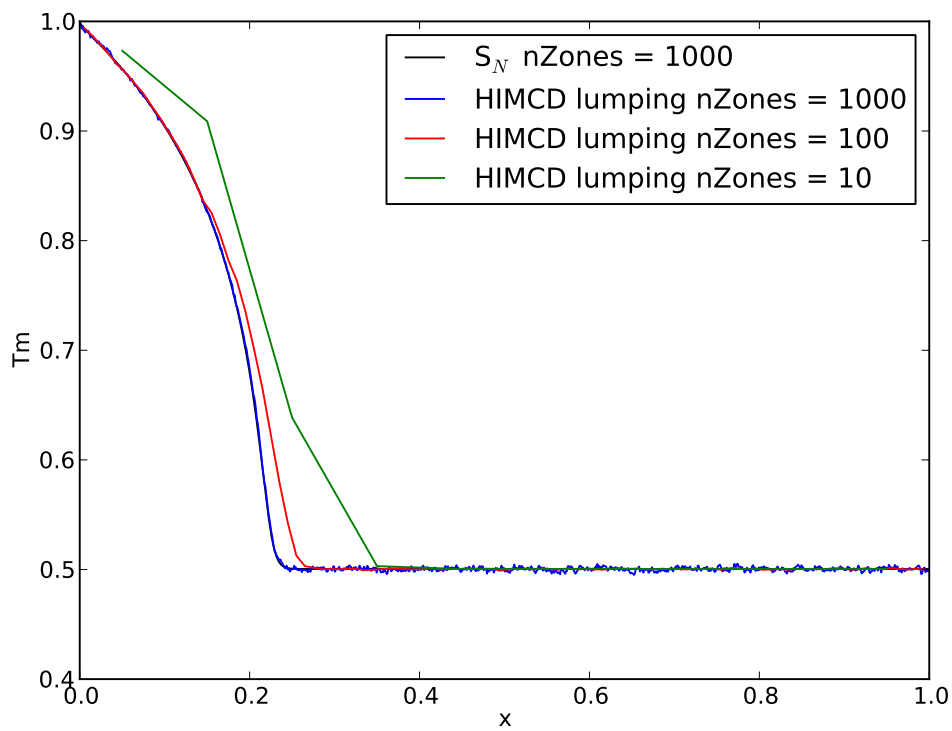


Figure 7: The HIMCD simulation results using source tilting for both the emission and up-scattering source in the heated iron test case at three different spatial refinements. The 10 zone spatial refinement is more accurate than the IMC result. However, up-scattering source teleportation error becomes significant in the intermediate refinement of 100 zones. In fact, the HIMCD result is actually less accurate than the IMC result for the 100 zone refinement.

The result of this requirement is that the zone optical thickness must be greater than about 4 mean free paths ( $\tau_{\min} \geq 4$ ) for a scattering ratio of 90% ( $\omega = 0.9$ ). This quickly limits the frequency groups that diffusion theory can be applied to in the HIMCD method. This limit directly corresponds to the interface condition and does not necessarily correlate to the accuracy of diffusion theory. There are however, some intuitive reasons to base the diffusion criterion on optical thickness and the scattering ratio other than this analytic limit. This is because it helps guarantee that photons will have many (isotropic) scattering collisions reducing the flux transients ( $\frac{\partial F}{\partial t}$ ) and making the photon intensity weakly dependent on angle (which are the assumptions that are required for diffusion theory).

We will now show that previous definitions of the diffusion criterion are more restrictive than necessary to produce an accurate result. In fact, we will show that by relaxing the diffusion criterion to include less opaque groups, it is possible to reduce the effects of up-scattering teleportation error. To understand the justification for relaxing the diffusion criterion, consider an ideal example of diffusion theory. This example consists of a semi-infinite slab of purely isotropic scattering material heated by a constant surface source. In this example, we would expect the photon intensity to be weakly dependent on angle and the derivative of the flux as a function of time to be small making it an ideal candidate for diffusion theory. However, if we continuously refine the spatial mesh that defines the slab we will eventually violate the minimum optical thickness requirement defined by Eq. 31 regardless of the validity of diffusion theory for the problem. It turns out that this limit is too restrictive because it is too local in scope, it only considers a single zone's properties. As it turns out the validity of diffusion theory has more to do with the global scope as opposed to the local scope of the problem. In contrary to this it is easy to see that relaxing the diffusion criterion too much can quickly cause problems in heterogeneous systems. Consider a very thin opaque material placed in between to optically thin materials. Even if the thin opaque material is highly scattering, it is likely not thick enough to produce enough scattering events to make the diffusion assumptions valid in the material. We therefore seek to relax the diffusion criterion in a way that captures more of the moderately opaque groups while maintaining a reasonable amount of local scope to prevent us from applying diffusion when it is not accurate.

#### 4.1. Modifying the diffusion-transport interface condition

In order to relax the diffusion criteria to include less opaque groups, it is necessary to modify the diffusion transport interface condition such that it ensures the probabilities will be bounded regardless of the zone's frequency-integrated optical thickness. To accomplish this, we modify the previously defined extrapolation distance when a zone is less than 4 mean free paths thick.

$$\lambda \begin{cases} 0.7104 & \text{if } \tilde{\kappa}_r \Delta x > 4 \\ \tilde{\lambda} & \text{else} \end{cases}$$

The modified extrapolation distance  $\tilde{\lambda}$  is determined using Eq. 31 and is a function of the optical thickness  $\tilde{\tau} = \tilde{\kappa}_r \Delta x$  and the scattering ration  $\tilde{\omega} = \frac{\tilde{\kappa}_r - f \tilde{\kappa}_p}{\tilde{\kappa}_r}$

$$\tilde{\lambda} = \frac{5}{3} + \frac{1}{\frac{3}{2}(1 - \tilde{\omega})\tilde{\tau} + \sqrt{3(1 - \tilde{\omega}) + \frac{9}{4}(1 - \tilde{\omega})^2\tilde{\tau}^2}} - \frac{1}{\sqrt{3(1 - \tilde{\omega})}}$$

The extrapolation distance  $\lambda$  is an empirical estimation of the location that the scalar intensity will diminish to zero assuming that it was linearly extrapolated away from the interface. This modified extrapolation distance is increased as the interface condition is applied to less optically thick zones. We assume that any additional errors associated with this modified interface condition are going to be less significant than the errors that occur from up-scattering teleportation error.

#### 4.2. The new diffusion criterion

The new diffusion criterion, which we will refer to as “over-lumping”, is constructed under the assumption that if a zone is reasonably opaque and the scattering ratio is high, then any group that significantly contributes to the effective scattering should be isotropic and Planckian. This new diffusion criterion is formed in two parts, one consisting of frequency integrated quantities, and the other of frequency-dependent quantities. The over-lumping diffusion criterion is easiest to express in pseudo code.

$$\gamma(v_g, \Delta x_z) \begin{cases} \text{if } \left( \frac{\kappa_r - f \kappa_p}{\kappa_r} < 0.9 \right) \\ \quad \text{return } \gamma = 0 \\ \text{else if } (\kappa_r \Delta x < 1.0) \\ \quad \text{return } \gamma = 0 \\ \text{else if } (\kappa_g \Delta x \geq 4) \\ \quad \text{return } \gamma = 1 \\ \text{else if } (\kappa_g \Delta x \geq 0.01 \ \&\& \ \xi_g \geq 1 \times 10^{-4} ) \\ \quad \text{return } \gamma = 1 \\ \text{else} \\ \quad \text{return } \gamma = 0 \end{cases}$$

The frequency integrated criteria are used such that diffusion is only applied in relatively opaque ( $\kappa_r \Delta x < 1.0$ ) highly scattering ( $\frac{\kappa_r - f \kappa_p}{\kappa_r} < 0.9$ ) zones. The frequency dependent criteria ensure that all opaque groups ( $\kappa_g \Delta x \geq 4$ ) in these zones are included and all moderately opaque groups ( $\kappa_g \Delta x \geq 0.01$ ) that significantly contribute to the effective scattering frequency spectrum ( $\xi_g \geq 1 \times 10^{-4}$ ). We call this an over-lumping diffusion criterion because we are include the moderately opaque groups that were previously treated as transport groups in the previous frequency-integrated (or “lumped”) hybrid methods defined by the diffusion criteria defined in Section 3.

#### 4.3. A demonstration of up-scatter source tilting and the over-lumping diffusion criterion

Figure 8 shows the temperature profile for the heated iron test case in Section 3.3 at the same spatial refinements using the new over-lumping criteria. Comparing Figures 7 and 8 shows that the new over-lumping approach significantly reduces the teleportation error, particularly in the 100 zone refinement which is no longer less accurate than IMC.

Figures 9 and 10 show the relative error of the material temperature as compared to the  $S_N$  solution at a 1000 zone refinement. Comparing these figures shows that over-lumping significantly improves the HIMCD results. This is particularly true for the 100 zone refinement which was being dominated by the up-scattering teleportation error in HIMCD with the old lumping diffusion criteria.

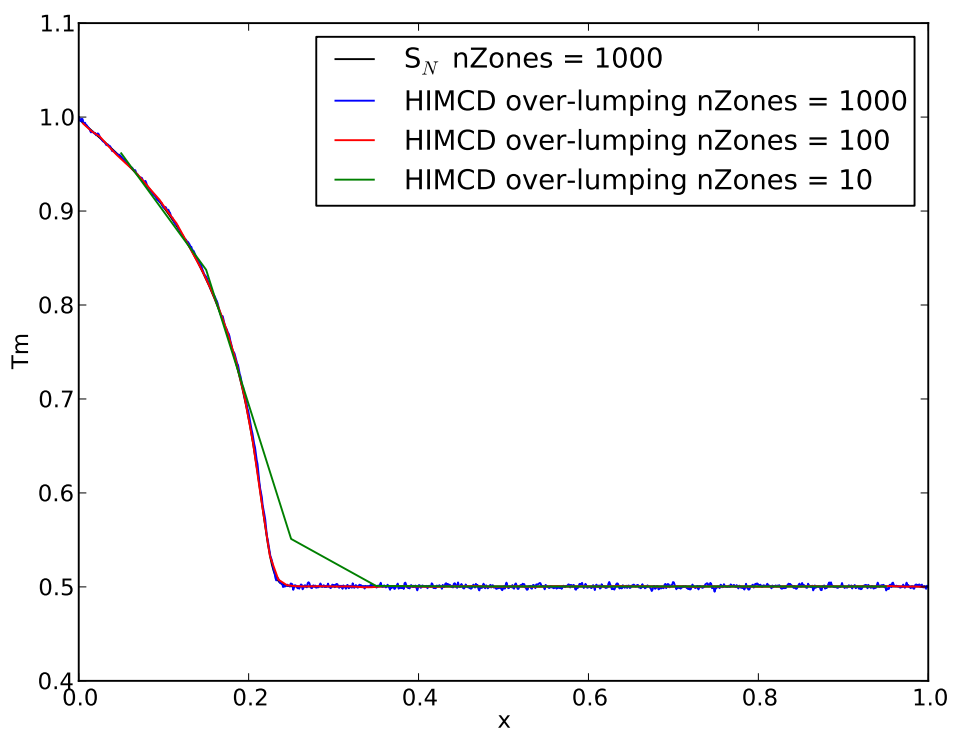


Figure 8: Using the over-lumping diffusion criteria, along with source tilting, significantly improves the results for the heated slab of iron at the 10 and 100 zone refinements.

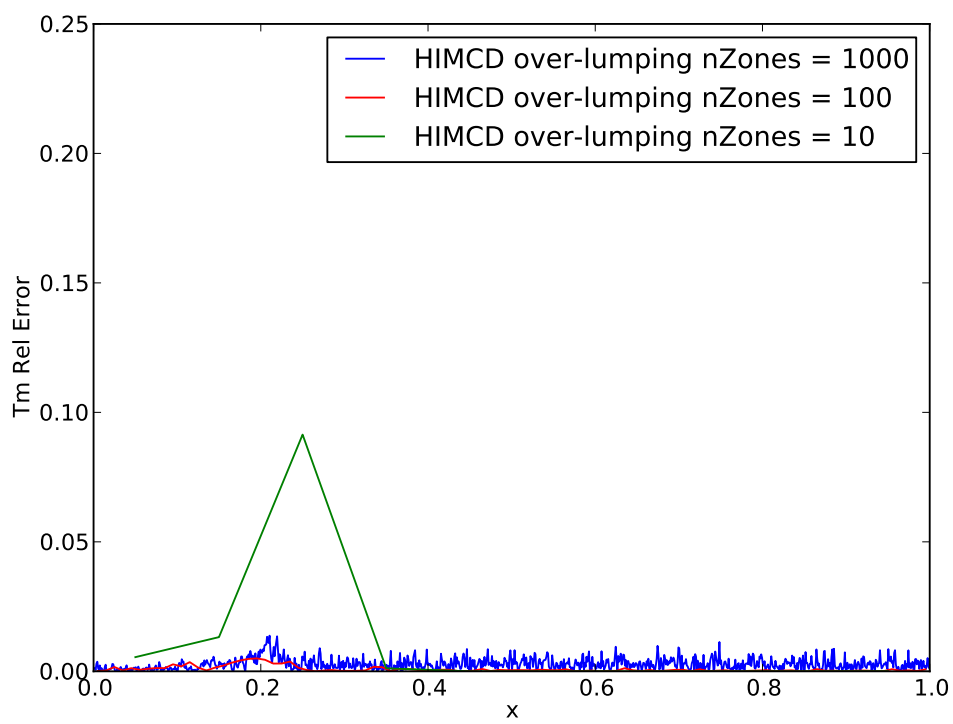


Figure 9: The relative error of the HIMCD method using up-scattering source tilting and over-lumping at the three different spatial refinements as compared to the 1000 zone  $S_N$ .

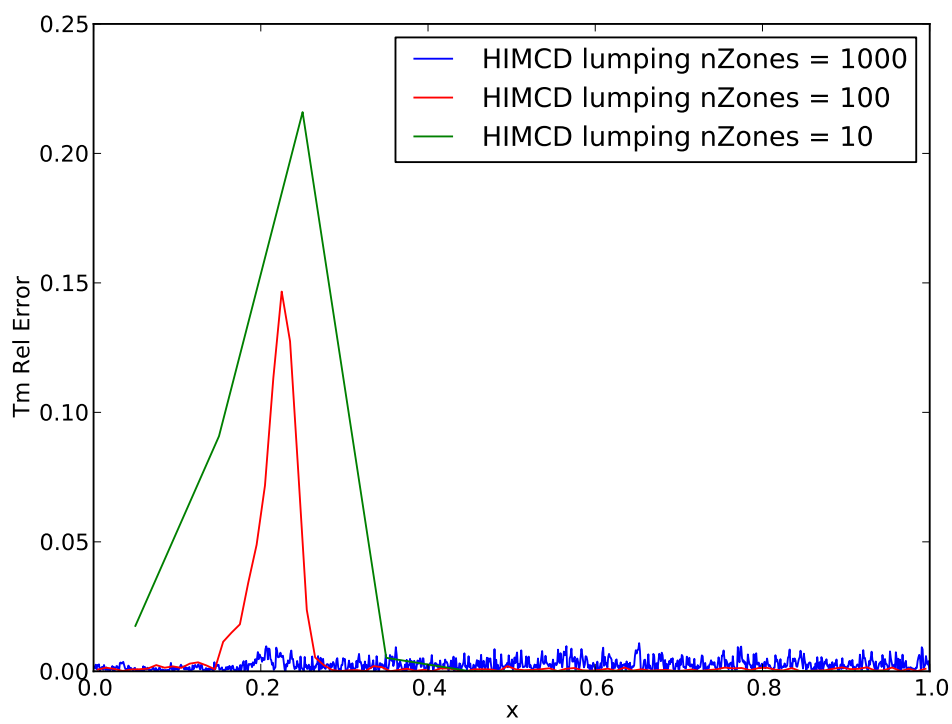


Figure 10: The relative error of the HIMCD method using up-scattering source tilting and the lumping diffusion criteria at the three different spatial refinements as compared to the 1000 zone  $S_N$ .

Table 1: Simulation run times, maximum relative error, and figure of merit for the various spatial refinements of the stationary heated iron test case.

# Zones	HIMCD over-lumping			HIMCD lumping			IMC		
	$t$ [s]	$\epsilon_{\max}$	$\eta$	$t$ [s]	$\epsilon_{\max}$	$\eta$	$t$ [s]	$\epsilon_{\max}$	$\eta$
10	7	0.091	1.57	12	0.22	0.38	805	0.344	0.004
100	87	0.005	2.30	87	0.15	0.08	804	0.036	0.03
1000	1105	0.014	0.06	1221	0.011	0.07	910	0.018	0.06

Table 1 lists the total simulation time  $t$ , the maximum relative error  $\epsilon_{\max}$ , and the figure of merit  $\eta = (t\epsilon_{\max})^{-1}$  for each of the simulations. All simulations were run using domain replication on 128 processors. The HIMCD algorithm takes slightly longer than IMC for the 1000 zone refinement because it performs extra work setting up the diffusion values which are not being used very often for the optically thin zones. The differences in run time have little effect on the overall figure of merit for the 1000 zone simulation.

#### 4.4. A radiation hydrodynamics example

To show the flexibility of the over-lumping diffusion criteria we will compare it to the standard lumping approach for a frequency-dependent radiation hydrodynamic simulation. The frequency-integrated HIMCD method presented here can easily be applied to the radiation hydrodynamic HIMCD originally presented for frequency-independent simulations by Cleveland et al.[7]. We will compare over-lumping to the standard lumping diffusion criteria using a simple ablation test case [7]. This test case consists of a block of optically thin silicon dioxide next to optically thick iron. A black body emission source is placed on the exterior face of the silicon dioxide. The radiation from the source streams through the silicon dioxide and deposits its energy into the optically thick iron. This causes the iron to rapidly expand creating a shock in both the iron and silicon.

The optically thick material, iron, spans the domain  $0 \leq x \leq 5$  [cm] and the optically thin material, silicon dioxide, spans the remainder of the spatial domain  $5 \leq x \leq 50$  [cm]. The iron is separated into 150 mesh zones which geometrically increase in size from the material interface at  $x = 5$  [cm] to  $x = 0$  [cm]. The silicon dioxide is composed of 50 spatial zones that geometrically increase in size from the material interface at  $x = 5$  [cm] to  $x = 50$  [cm]. The material starts at an initial temperature of  $T = 0.1$  [keV] and is heated during the simulation by a  $T_s = 1.0$  [keV] isotropic radiation source incident on the right side of the thin material at  $x = 50$  [cm]. The relationship between the change in material energy to the change in material temperature (Eq. 3) is evaluated using the Livermore equation of state database for iron and silicon dioxide. The iron is given an initial density of  $\rho_{\text{Fe}} = 7.86$  [g/cc] and the silicon dioxide is given an initial density of  $\rho_{\text{SiO}_2} = 2.65 \times 10^{-4}$  [g/cc]. The simulation was evaluated from the initial time  $t = 0$  to a final time  $t = 1 \times 10^{-7}$  [sec] using a maximum time step size of  $1 \times 10^{-10}$  [sec]. Each method used  $1 \times 10^7$  Monte Carlo particles per time step. We applied a frequency stencil of 30 logarithmically spaced frequency groups ( $1e-3 < \nu < 100.0$ ) [keV] for every simulation.

Figures 11, 12, 13, and 14 show the velocity ( $u$ ), density ( $\rho$ ), material temperature ( $T_m$ ), and radiation temperature ( $T_r$ ) profiles as evaluated by  $S_N$  and HIMCD using

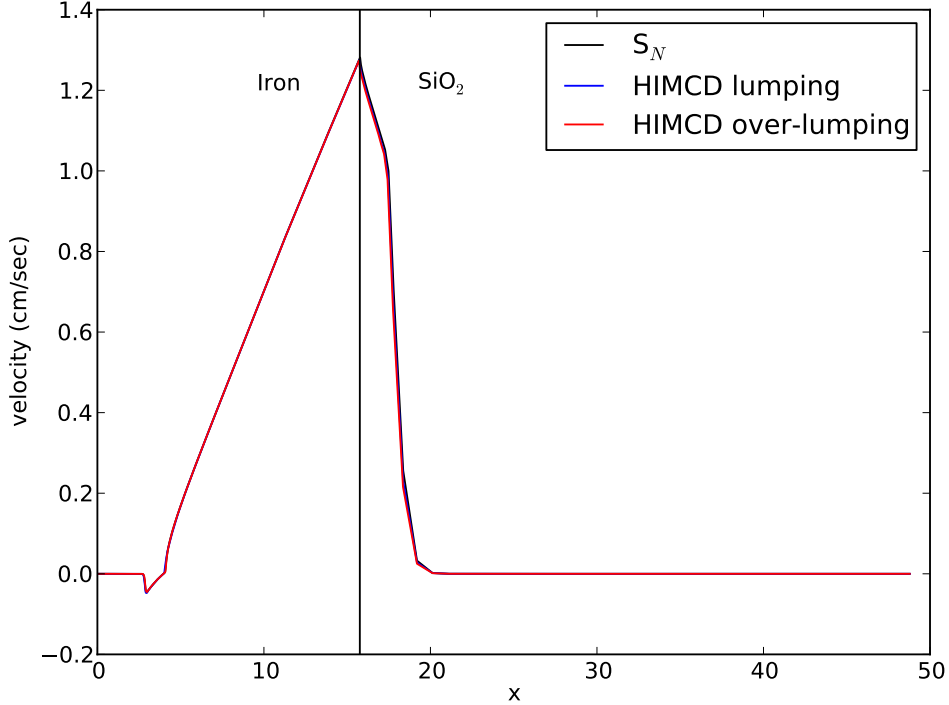


Figure 11: The velocity profile for HIMCD using lumping and over-lumping compared to the  $S_N$  solution.

lumping and over-lumping. The  $S_N$  solution is used as the reference result to generate relative errors comparing the two methods.

Figures 15, 16, 17, and 18 show the absolute error of the velocity<sup>1</sup>, the relative error of the density, material temperature, and radiation temperature for each of the HIMCD simulations as compared to the  $S_N$  reference solution. These figures show that the over-lumped HIMCD method agrees better with the  $S_N$  solution in the optically thick material, while the standard lumped HIMCD method agrees better in the optically thin material.

Table 2 lists the run times for each of the simulations, the maximum relative error, and the figure of merit. The most substantial difference is that over-lumping reduces the maximum relative error in the material density, as compared to the  $S_N$  reference solution, by nearly an order of magnitude. The other quantities appear to be less sensitive to the over-lumping as compared to the standard lumping approach.

## 5. Conclusions

In this work we have shown that frequency-dependent HIMCD, and similarly Hybrid DDMC, suffer from a new kind of source teleportation error. This new teleportation error

<sup>1</sup>Absolute error is used for the velocity values, rather than relative error, because they are near zero.

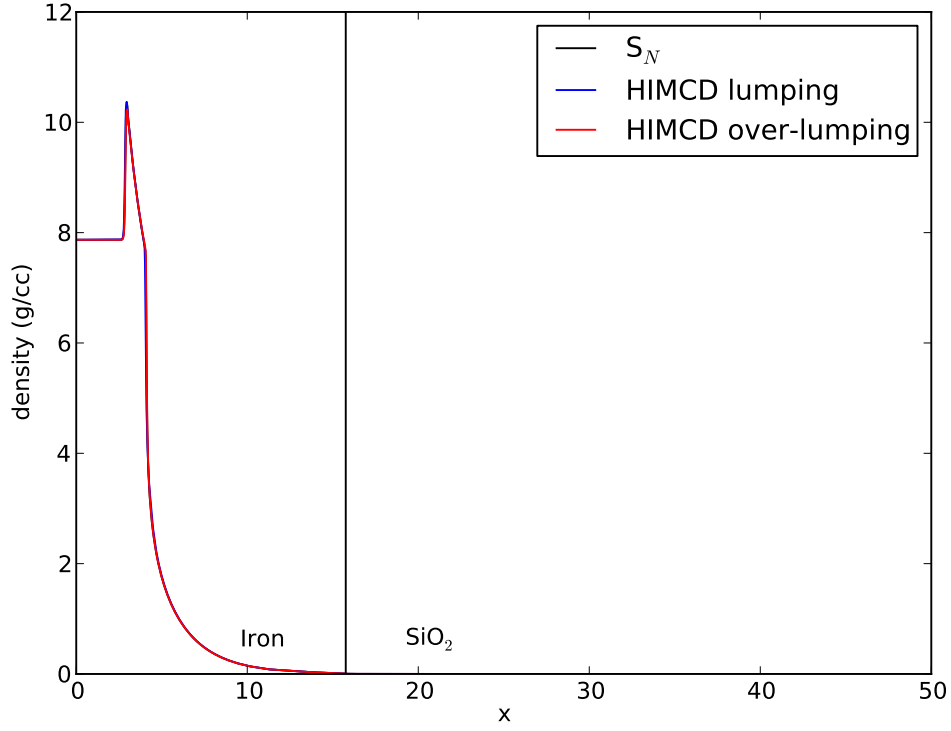


Figure 12: The density profile for HIMCD using lumping and over-lumping compared to the  $S_N$  solution.

Table 2: Simulation run times, maximum relative error, and figure of merit for the simple frequency dependent ablation test case.

Variable	HIMCD over-lumping			HIMCD lumping		
	$\tau$ [s]	$\epsilon_{\max}$	$\eta$	$\tau$ [s]	$\epsilon_{\max}$	$\eta$
$\rho$	2020	0.08	0.006	2328	0.32	0.001
$u$		0.05 <sup>1</sup>	0.010		0.03 <sup>1</sup>	0.014
$T_r$		0.04	0.012		0.16	0.003
$T_m$		0.15	0.003		0.15	0.003

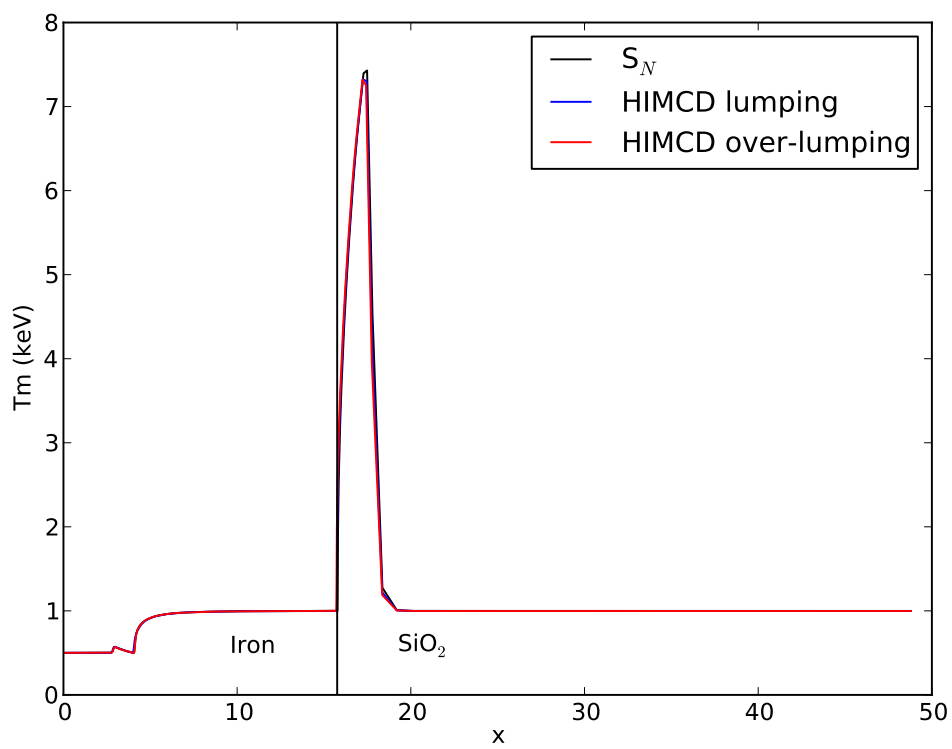


Figure 13: The material temperature profile for HIMCD using lumping and over-lumping compared to the  $S_N$  solution.

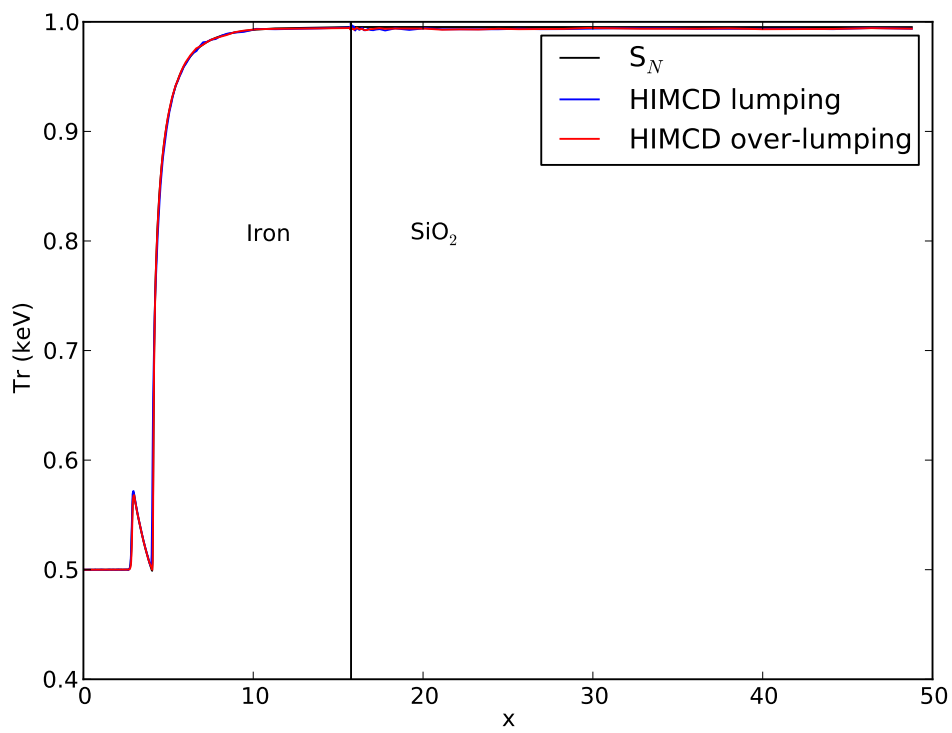


Figure 14: The radiation temperature profile for HIMCD using lumping and over-lumping compared to the  $S_N$  solution.

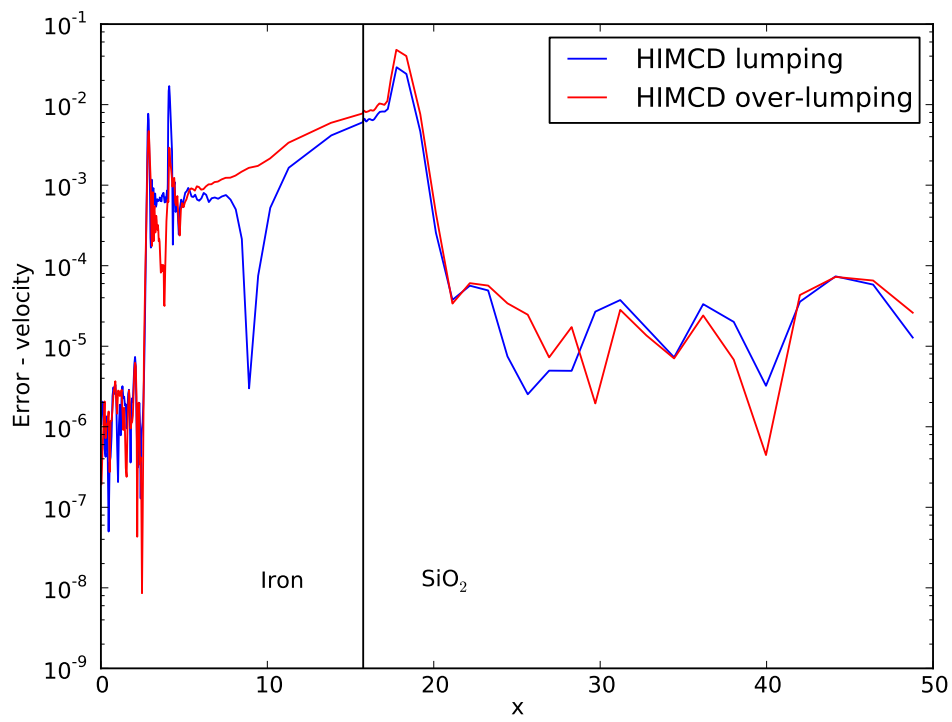


Figure 15: The absolute error of the velocity profile for HIMCD using lumping and over-lumping compared to the  $S_N$  solution.

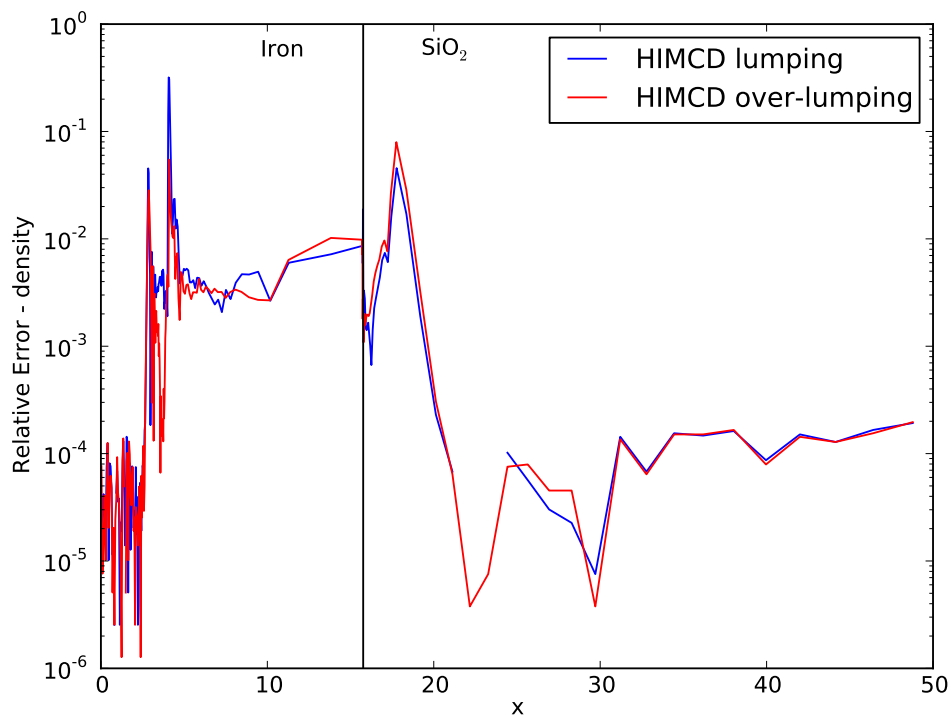


Figure 16: The relative error of the density profile for HIMCD using lumping and over-lumping compared to the  $S_N$  solution.

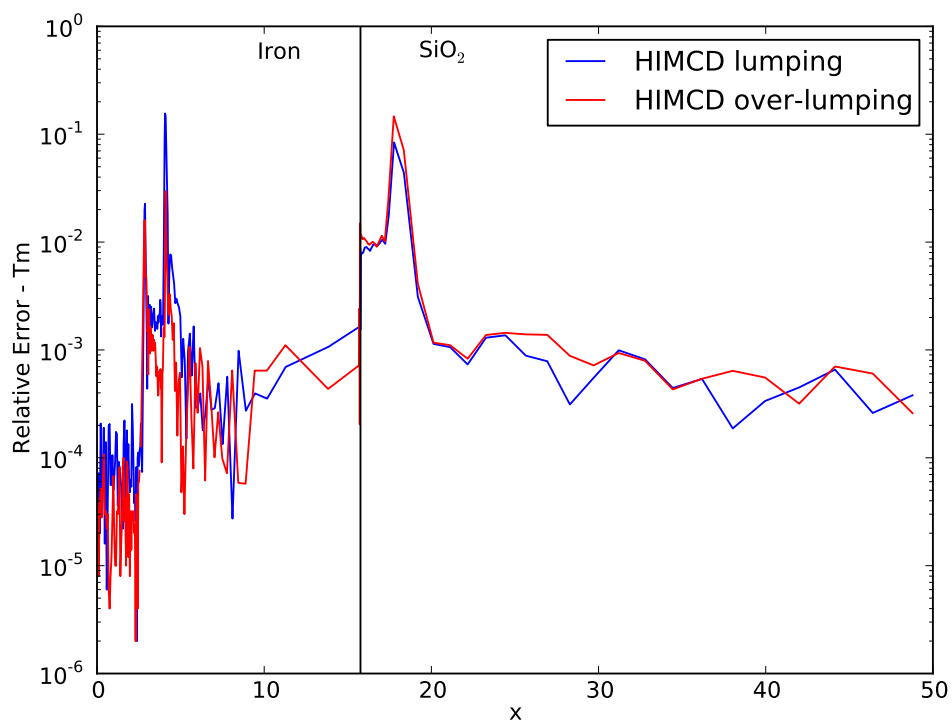


Figure 17: The relative error of the material temperature profile for HIMCD using lumping and over-lumping compared to the  $S_N$  solution.

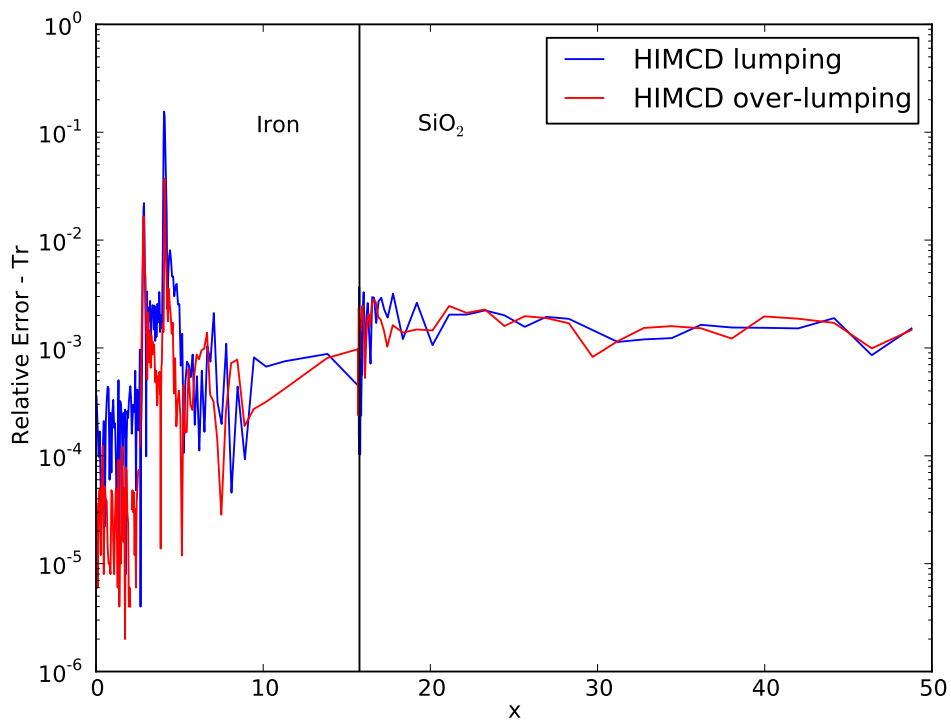


Figure 18: The relative error of the radiation temperature profile for HIMCD using lumping and over-lumping compared to the  $S_N$  solution.

arises from using poor spatial shapes to represent the discrete events when particles scatter from the diffusion to the transport domain.

We found that source tilting significantly reduces the up-scattering teleportation error in moderately opaque problems. This is because source tilting better represents the true spatial distribution of the up-scattering events as compared to a piecewise constant distribution. We found that our source tilting scheme was not enough to completely prevent a significant amount of teleportation error from accumulating.

Finally, we show that up-scattering teleportation error can be significantly reduced, even in very optically thick materials, by lumping the previously excluded moderately opaque opacity groups into the diffusion domain. This over-lumping was accomplished by modifying the diffusion criterion to be based on both frequency-integrated and frequency-dependent quantities.

A consequence of including the moderately opaque groups was that we had to modify the diffusion-transport interface condition to accommodate zones of arbitrary optical thicknesses. The errors associated with this modified interface conditions were shown to be less impactful than the improvements in the reduction of teleportation error.

The frequency-integrated over-lumped HIMCD method, which uses source tilting to sample the spatial locations of up-scattering, was significantly more accurate than the standard frequency-integrated HIMCD method previously presented. In fact, we showed that the HIMCD method is not just faster than IMC, but is also more accurate in very opaque materials. The new over-lumping and source tilting schemes eliminate the majority of the emission and up-scattering teleportation error regardless of the overall optical density of the problem.

## Acknowledgments

This work performed under the auspices of the U.S. Department of Energy by Lawrence Livermore National Laboratory under Contract DE-AC52-07NA27344.

## References

- [1] N. A. Gentile, Implicit monte carlo DiffusionAn acceleration method for monte carlo time-dependent radiative transfer simulations, *Journal of Computational Physics* 172 (2001) 543–571.
- [2] M. A. Cleveland, N. A. Gentile, T. S. Palmer, An extension of implicit monte carlo diffusion: Multigroup and the difference formulation, *Journal of Computational Physics* 229 (2010) 5707–5723.
- [3] J. Fleck Jr., J. Cummings Jr., An implicit monte carlo scheme for calculating time and frequency dependent nonlinear radiation transport, *Journal of Computational Physics* 8 (1971) 313–342.
- [4] M. S. McKinley, E. D. Brooks III, A. Szoke, Comparison of implicit and symbolic implicit monte carlo line transport with frequency weight vector extension, *Journal of Computational Physics* 189 (2003) 330–349.
- [5] J. D. Densmore, K. G. Thompson, T. J. Urbatsch, A hybrid transport-diffusion monte carlo method for frequency-dependent radiative-transfer simulations, *Journal of Computational Physics* 231 (2012) 6924–6934.
- [6] R. T. Wollaeger, D. R. van Rossum, C. Graziani, S. M. Couch, G. C. Jordan IV, D. Q. Lamb, G. A. Moses, Radiation Transport for Explosive Outflows: A Multigroup Hybrid Monte Carlo Method, arXiv e-print 1306.5700, 2013.
- [7] M. Cleveland, N. Gentile, Using hybrid implicit monte carlo diffusion to evaluate the frequency-independent radiation hydrodynamic equations, *Journal of Computational Physics* (Submitted 2013).
- [8] J. D. Densmore, Asymptotic analysis of the spatial discretization of radiation absorption and re-emission in implicit monte carlo, *Journal of Computational Physics* 230 (2011) 1116–1133.
- [9] N. A. Gentile, N. Keen, J. Rathkopf, The Kull IMC package, Technical Report UCRL-JC-132743, Lawrence Livermore National Laboratory (LLNL), Livermore, CA, 1998.

- [10] R. H. Szilard, G. C. Pomraning, Numerical transport and diffusion methods in radiative transfer, 1992.
- [11] J. D. Densmore, Interface methods for hybrid monte carlo-diffusion radiation-transport simulations, *Annals of Nuclear Energy* 33 (2006) 343–353.
- [12] M. F. Modest, Radiative heat transfer, Academic Press, 2003.
- [13] T. J. Urbatsch, T. M. Evans, Milagro Version 2 an Implicit Monte Carlo Code for Thermal Radiative Transfer: Capabilities, Development, and Usage, Technical Report LA-14195-MS, Los Alamos National Laboratory (LANL), Los, Alamos, NM, 2006.
- [14] J. D. Densmore, G. Davidson, D. B. Carrington, Emissivity of discretized diffusion problems, *Annals of Nuclear Energy* 33 (2006) 583–593.